RSC Advances

PAPER

View Article Online
View Journal | View Issue

CrossMark click for updates

Cite this: *RSC Adv.*, 2015, **5**, 586

Substitution effect on chalcone based materials for corrosion and photocrosslinking applications†

V. Ramkumar,[a] S. Anandhi,[b] P. Kannan[a] and R. Gopalakrishnan*[c]

Received 21st September 2014
Accepted 14th November 2014

DOI: 10.1039/c4ra10884a

www.rsc.org/advances

Three different substituted novel chalcone based materials namely (*E*)-3-(4-(benzyloxy)phenyl)-1-(4-hydroxyphenyl)prop-2-en-1-one (chalcone **I**), (*E*)-1-(4-(benzyloxy)phenyl)-3-(4-hydroxyphenyl)prop-2-en-1-one (chalcone **II**) and (*E*)-1,3-bis(4-(benzyloxy)phenyl)prop-2-en-1-one (chalcone **III**) were designed and synthesized by a standard Claisen–Schmidt condensation reaction. The different surface morphologies of these materials were obtained from SEM (Scanning Electron Microscopy) analysis. Single crystal XRD studies of chalcone **III** indicate a monoclinic system with a space group of $P2_1/c$. Thermal studies such as TGA, DSC and HOPM revealed good thermal stability, crystallinity and phase changing properties of material **III**. The HOMO, LUMO and bandgap energies of these three materials were calculated by theoretical (DFT) calculations. The electrochemical analysis involves Tafel plots and cyclic voltammetry studies to demonstrate high corrosion inhibition percentage and oxidation–reduction behaviour of materials **I**, **II** and **III**. Dissimilar photocrosslinking time of all three materials was obtained from micro photo-reactor and UV-visible spectrophotometry. The comparative and structural linearity statement reveals the outline view property of the similar chalcone families.

Introduction

Chalcone based materials play an important role in upcoming research fields,[1–3] since they have the push–pull conjugation effect and α,β-unsaturated ketone group present in the material.[4] The special intra charge transfer (ICT) leads to delocalization of electrons within the chalcone molecule.[5] The electron withdrawing and accepting groups in this type of chalcone molecule leads to a drastic change in behaviour and has been used in industry for various application.[4] The chalcone core crystals find a place in optics, communications, liquid crystals and frequency modulation.[6–8] The chalcone nonlinear optical materials are expected to be dynamic for optical communication and opto-electronics because of their applications in high-speed and high-density data processing.[9–11] Second order nonlinear optical materials were used in optical switching, frequency conversion and electro-optical applications.[12] It has been generally understood that the second-order molecular nonlinearity can be enhanced by large delocalized π-electron systems with strong donor and acceptor groups.[13]

Corrosion is an important task to handle in solving problems, because the loss of metals is increasing with respect to corrosive nature.[14] Some chalcones act as a good inhibitor for the corrosion science.[15] Substituting suitable compounds into the metals as coating or painting or some other forms to metal surface inhibits corrosive nature of the metal.[16] The addition of various compounds make as less oxidative nature to metal surface and atmospheric oxygen.[14] It is inferred from the previous reports that hydroxyl substituted chalcone compounds are giving good inhibiting nature.[17]

On the other hand, among many organic compounds are reported for their photocrosslinking, chalcone derivatives exhibits excellent photocrosslinking nature due to the presence of α,β-unsaturated ketone group.[18,19] Since the conjugated double bonds of enone moiety involves photocrosslinking changes. In addition, chalcone based materials also useful in biological field. The presence of α,β-unsaturated compounds leads to have variety of medicinal purposes such as antibacterial, anticancer, antimalarial, anti-inflammatory, antifungal, and anti-tumor.[20,21]

The objective of this present investigation is about synthesis and characterization of three different substituted new chalcone based materials (Fig. 1). The physico chemical properties and theoretical analysis of these three materials were subjected to different characterization techniques such as TGA, DSC, HOPM, SEM, cyclic voltammetry and DFT analysis. The rate of corrosion and the rate of photocrosslinking of these three

[a]*Department of Chemistry, Anna University, Chennai-25, India*
[b]*Department of Physics, Maamallan Institute of Technology, Sriperumpudhur, Chennai, 602105, India*
[c]*Crystal Research Laboratory, Department of Physics, Anna University, Chennai-25, India. E-mail: krgkrishnan@annauniv.edu; krgkrishnan@yahoo.com*

† Electronic supplementary information (ESI) available: The harvested crystal image (Fig. S1), FT-IR data of intermediate and final product of chalcone **III** is shown Fig. S2, ORTEP diagram of chalcone **I**, **II**, **III**, Fig. S3, hydrogen bonding coordinates data of crystal **III** (Table S1), video clip of isotropic state to cooling crystalline state is also available. CCDC 909642. For ESI and crystallographic data in CIF or other electronic format see DOI: 10.1039/c4ra10884a

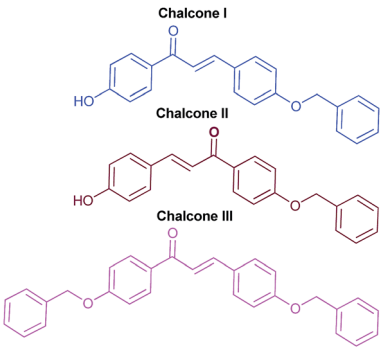

Fig. 1 The molecular structure of chalcone I, II and III.

materials were evaluated using electrochemical analyser and micro photo reactor and UV-visible spectrophotometer.

Experiments and characterization

Materials

All the chemicals such as benzyl chloride, 4-hydroxybenzaldehyde, 4-hydroxyacetophenone, potassium carbonate (K_2CO_3), potassium iodide (KI), sodium hydroxide (NaOH), ethanol, DMF and acetone and other precursors were procured from Sigma Aldrich (USA).

Synthesis of materials

The chalcone **I** and **II** were synthesized by adopting Claisen–Schmidt condensation reaction and chalcone **III** synthesized by similar method from the intermediate derivatives of respective aldehyde and ketone as follows.[4] Equimolar quantities (0.01 mol each) of the intermediate product of compound **I** (4-(benzyloxy)benzaldehyde) and compound **II** (4-(benzyloxy)acetophenone) were stirred in ethanol (60 mL) for about 30 min. Aqueous solution of sodium hydroxide (0.02 mol, 5 mL, 10%) was added very slowly drop wise while stirring. The reaction mixture was poured into ice cold water (300 mL) and left for 10 h and obtained yellow colour precipitate. The resulting solid product was obtained from filtration, dried and further purified two times using ethanol by repeated recrystallization. Material **III**: yield: 85%; mp 147 °C. FT-IR (KBr) (cm^{-1}): 2875 (C–H) aliphatic, 1670 (C=O), 1100 (C–O). ^{1}H-NMR (Fig. 2) (500 MHz, $CDCl_3$) (δ/ppm): 5.18 (s, 2H, Ar-CH_2); 7.05 (d, 1H, Ar-CH); 7.09 (d, 1H, Ar-CH); 7.36 (m, 1H, Ar-H); 7.42 (m, 1H, Ar-CH); 7.61 (d, 1H, Ar-H); 7.62 (d, 1H, Ar-H); 7.80 (d, 1H, Ar-H); 8.06 (d, 1H, Ar-H) (Scheme 1).

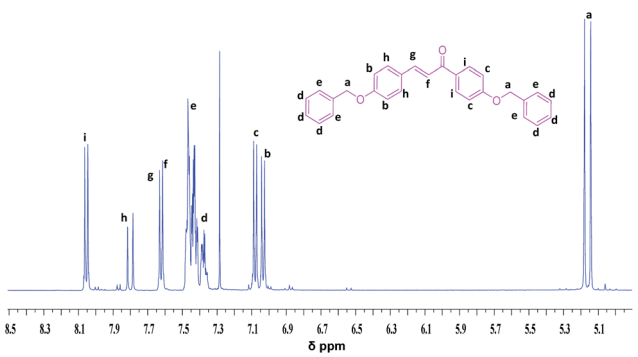

Fig. 2 ^{1}H-NMR spectrum of chalcone III.

Crystal growth

Dichloromethane was found to be the suitable solvent for single crystal growth of material **III**, whereas acetone was accomplished as preferred solvent for crystallization of **I** and **II**.[4] This different recrystallization solvent is due to the absence of –OH group leads to less hydrogen bonding in material **III**. The fully saturated solution of material **III** in the dichloromethane is stirred at ambient temperature for 1 h. Then the solution was filtered, slightly warmed and allowed to evaporate very slowly at room temperature. After 5 days, good quality seed crystals were observed to a dimension of 15 mm × 12 mm × 5 mm. The grown crystals are shown in Fig. S1.†

Measurements

High-resolution ^{1}H-NMR spectrum of the compound was recorded on a 500 MHz AVANCE III spectrometer in $CDCl_3$ with TMS as an internal standard. The Fourier Transform Infrared (FT-IR) spectra of respective aldehyde, ketone and material **III** were recorded between the regions of 600 to 4000 cm^{-1} using a Bruker IFS 66V Fourier transform spectrometer and shown in Fig. S2.† Thermo gravimetric analysis (TGA) was performed on a Mettler TA3000 thermal analyser under nitrogen atmosphere at a heating rate of 5 °C min^{-1} with a sample weight of 3–5 mg. DSC measurements were performed on a Mettler Toledo STARe system to scan the synthesized material in unsealed alumina pan in a dry nitrogen atmosphere with an empty aluminium pan as a reference. The scans were carried out at a heating rate of 5 °C min^{-1}. Hot stage optical polarized microscopy (HOPM) studies were made on a Euromax polarizing optical microscope equipped with a Linkem HFS-91 heating stage and a TP-93 temperature programmer. Small quantity of material was

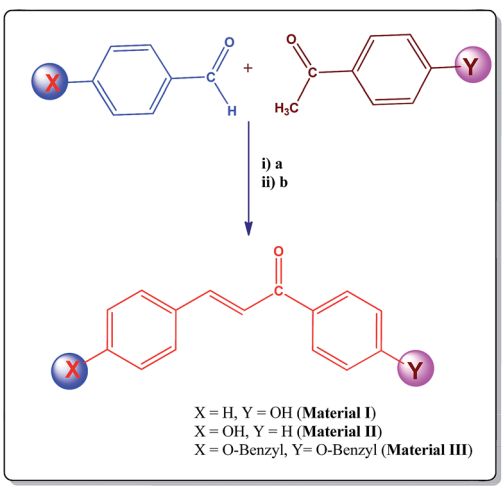

Scheme 1 (i) a = EtOH/NaOH and (ii) b = 6 hours per 10 °C.

placed between two thin glass cover slips, heated and cooled at the rate of 5 °C min^{-1}. The phase change on heating of crystal was observed and photographs taken on a Canon EOS 1000D camera.

Single crystal X-ray diffraction

The obtained structural configuration of materials **I**, **II** and **III** were been as (*E*) configuration has confirmed from single crystal XRD diffraction (ORTEP Diagram) as shown in Fig. S4.† Intensity data for crystal **III** was collected at room temperature for a crystal dimension of 0.35 × 0.25 × 0.2 mm^3 using a Bruker AXS Kappa APEX II single crystal CCD diffractometer equipped with graphite-monochromated MoKα radiation (λ = 0.71073 Å). The unit cell parameters were determined from 36 reflections measured along the three different crystallographic zones by the method of difference vectors. The data collection, reduction and absorption correction were performed by APEX2, SAINT-plus and SADABS program.[4]

The structure was solved by direct method and non-hydrogen atoms subjected to anisotropic refinement by full-matrix least squares on F^2 using SHELXL-97 program.[4] The positions of all the hydrogen atoms were identified from different electron density map and constrained to ride on the corresponding non-hydrogen atoms. The hydrogen atom bound to carbon atoms were constrained to a distance of C–H = 0.93–0.97 Å and $U_{iso(H)} = 1.2U_{eq(C)}$ and $1.5U_{eq(C)}$. The hydrogen atom associated with oxygen atom was allowed to ride on the parent atom with a distance of 0.82 Å and $U_{iso(H)} = 1.5U_{eq(C)}$.

Electrochemical analysis

Preparation of mild steel specimens and electrolytes

CH electrochemical analyser model 604B was used to record Tafel polarization curve. The mild steel having compositions of C = 0.22%, Mn = 0.22%, Zn = 0.22% and Fe = 99.34% were procured and used for further analysis. A conventional three-electrode system was used for this analysis.[22] Mild steel specimen of an exposed area of 1 cm^2 was used as a working electrode. Pt and SCE were used as auxiliary and reference electrodes, respectively. The working electrode was polished with a series of emery papers from 400 to 1200 grade and washed thoroughly with double distilled water, degreased with acetone and then air dried. The concentration range of inhibitors employed was varied from 10 to 100 ppm and the electrolyte used was 100 mL per experiment. The solutions were prepared by dilution of analytical grade 37% HCl with double distilled water in the absence and presence of inhibitors. The potentiodynamic polarization curves were recorded by changing electrode potential *versus* the open-circuit potential (OCP) with a scan rate of 20 mV min^{-1}. The linear Tafel segments of the anodic (ba) and cathodic (bc) curves were extrapolated to the corrosion potential to obtain corrosion current densities (I_{corr}).

Cyclic voltammetry measurements were performed on a CHI 600D electrochemical analyser at room temperature with three electrode cell in a solution of Bu_4NClO_4 (0.1 M) in dichloromethane at a scanning rate of 100 mV s^{-1}. GC electrode was used as working electrode and a platinum foil was used as a counter electrode and Ag/AgCl electrode was used as reference electrode.[23] Reference electrode was calibrated after each measurement using ferrocene (Fc).

Photocrosslinking studies

The UV-visible spectrophotometer SHIMADZU UV-1650PC and microwave photo reactor (Heber micro photo reactor) were used to analyse the photocrosslinking of all the three materials. Typical procedure was adopted for photo-isomerization process as follows: chalcone materials were subjected to UV-irradiation starting from a 125 W pressure mercury lamp (365 nm) kept at a distance of 10 cm from a sample at various intervals of time followed by UV absorption measured on the spectrophotometer respectively.[24] This procedure was repeated until reduction in absorption was completed.

Results and discussion

Single crystal X-ray diffraction

The crystalline structure and physical properties of materials **I** and **II** were reported in the previous work[4] and the new material **III** crystal structure and properties were analysed and reported in the present investigation.† Single crystal XRD data of material **III** exhibit the liberal packing of the system. Since there is a weak hydrogen bonding in this material, the packing lies to form a layer like structure. Fig. 3 demonstrates that various packing alignment of crystal **III**. Table 1 provide the crystal data for **III**. The material **III** crystallizes in centrosymmetric monoclinic crystal system with space group of $P2_1/c$.

Morphology

The morphology of the crystal **III** can be simulated from powder X-ray diffraction pattern using WinXMorph (Version 1.0, Release 4, Build 6) software and is shown in Fig. 4. The generated morphology view of the crystal was found to be similar, indicating block morphology. The grown crystal and derived structure of the crystal are the same shape.

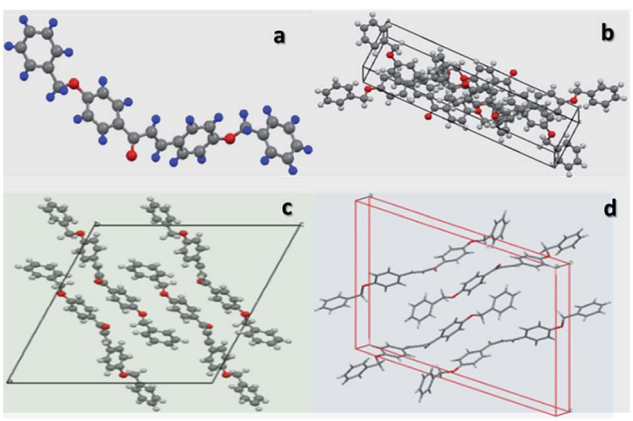

Fig. 3 (a) ORTEP diagram. (b) Packing alignment along *b* axis. (c) Different packing alignment of crystal III.

Table 1 Single crystal XRD data of chalcone crystal III

Identification code	Crystal **III**
Empirical formula	$C_{29}H_{24}O_3$
Formula weight	420.48
Temperature	296(2) K
Wavelength	0.71073 Å
Crystal system, space group	Monoclinic, $P2_1/c$
Unit cell dimensions	$a = 22.855(3)$ Å, $\alpha = 90^\circ$
	$b = 5.7603(5)$ Å, $\beta = 109.164(3)^\circ$
	$c = 17.5590(18)$ Å, $\gamma = 90^\circ$
Volume	2183.6(4) Å^3
Z, calculated density	4, 1.279 Mg m^{-3}
Absorption coefficient	0.082 mm^{-1}
F(000)	888
Crystal size	0.35 × 0.30 × 0.25 mm^3
Theta range for data collection	2.32 to 21.11°
Limiting indices	$-23 \le h \le 23$, $-5 \le k \le 5$, $-17 \le l \le 17$
Reflections collected/unique	12 760/2360 [$R_{(int)} = 0.0410$]
Completeness to theta = 21.11	99.7%
Absorption correction	Semi-empirical from equivalents
Max. and min. transmission	0.9799 and 0.9020
Refinement method	Full-matrix least-squares on F^2
Data/restraints/parameters	2360/0/290
Goodness-of-fit on F^2	1.095
Final R indices [I > 2sigma(I)]	$R_1 = 0.0461$, w$R_2 = 0.1038$
R Indices (all data)	$R_1 = 0.0609$, w$R_2 = 0.1105$
Extinction coefficient	0.0014(4)
Largest diff. peak and hole	0.330 and −0.119 e A^{-3}

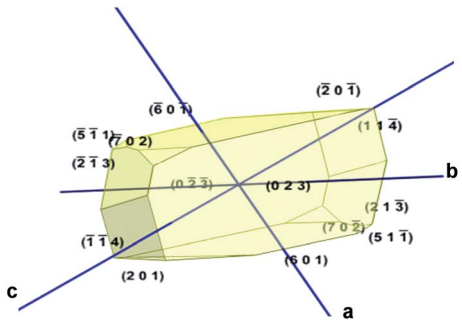

Fig. 4 Virtual morphology of chalcone III.

Hardness

Hardness test discloses the mechanical behaviour of the materials.[4] Hardness is the resistance offered by a material for the applied load. The micro hardness test was performed using MATZUKA Vickers micro hardness tester attached with diamond pyramidal indenter and microscope. Fig. 5 exhibits the hardness behaviour of crystal **III**. At very low load, hardness is high,[25] on increasing the applied load, hardness decreases the phenomenon is termed as indentation size effect.[26] while increasing load the hardness value decreases owing to reverse indentation size effect. Meyer's index reveals that the above said chalcone crystal belongs to the soft material category. Hardness is calculated using the following eqn (1).[4]

$$H_v = \frac{1.8544P}{d^2}\left(\text{kg mm}^{-2}\right) \quad (1)$$

where, H_v = hardness number, P = applied load, d = indentation size.

The experiment is repeated 3 times and error bar is plotted between the applied load and hardness number. Hardness plot infers that crystal withstands only lower loads indicating the mechanical stability of the grown chalcone crystal.

Thermal properties of the material

The thermal stability of material **III** was studied by TGA analysis. The result was shown in Fig. 6 and proved that the crystal is stable up to 345 °C and decomposes at 800 °C. The char yield of

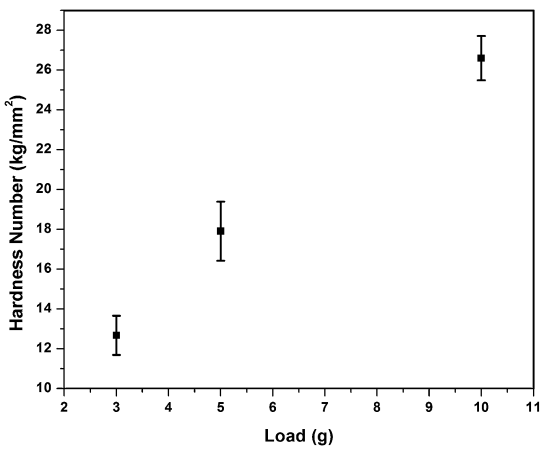

Fig. 5 Hardness plot of chalcone crystal III.

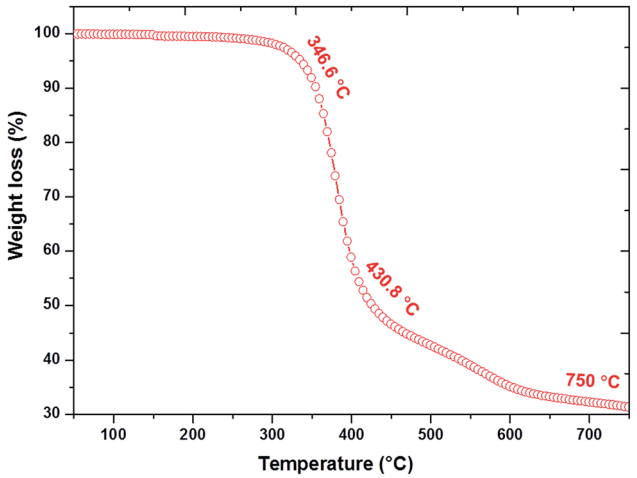

Fig. 6 TGA curve of chalcone III.

material was observed at 7.64%. The DSC curve (Fig. 7) displays a sharp exothermic peak at 147 °C which implies that material **III** has a sharp melting point at 147 °C. This sharp peak enumerates the evidence that the compound exhibit high crystalline nature. The cooling curve of the endothermic peak displays that the compound has a tendency to crystalize while cooling at 120 °C.

Hot stage optical polarized microscope (HOPM) deals about thermal properties and phase changes of crystalline to isotropic and isotropic to crystalline state of material **III**.[4] In particular, physical change on heating and accurate melting point of the materials could be obtained from HOPM analysis. Fig. 8 illustrates the HOPM analysis result of material **III**. It reveals that crystal **III** has a sharp melting point (crystalline to isotropic) at 147 °C and cooling crystallization (isotropic to crystalline) of the chalcone occurs at 120 °C while cooling the first cooling reveals a needle like image indicating that the material has highly crystalline nature. Further second heating and cooling shows

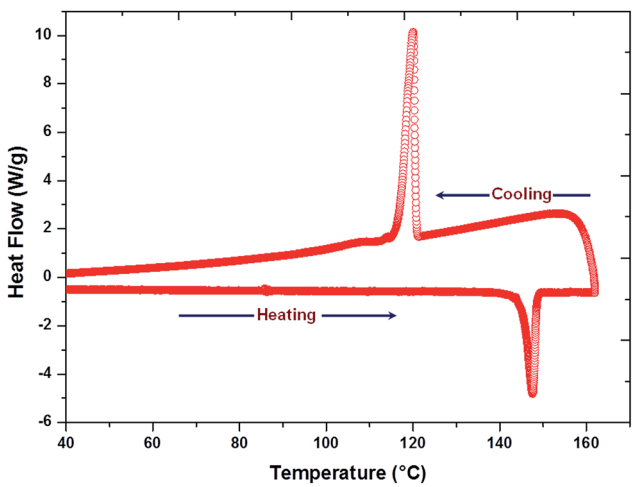

Fig. 7 DSC traces of chalcone III.

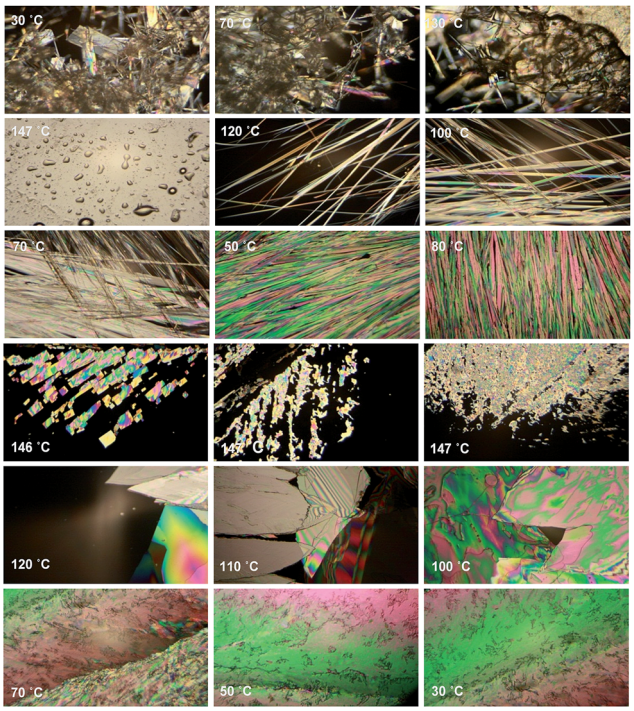

Fig. 8 HOPM heating and cooling cycle images of material III at various temperatures, crystalline to isotropic (30 °C to 147 °C), isotropic to crystalline (147 °C to 50 °C). Further heating on crystalline to isotropic (50 °C to 147 °C), cooling on isotropic to crystalline (147 °C to 30 °C).

the same melting and cooling point which match with the first one (Video has been attached†).

The sharp edge and needle like images exhibit that material **III** has highly crystalline in nature. The cooling phase and the room temperature images also imply the good crystalline nature of the material **III**. The image evinces the smooth morphology of material **III**. The obtained HOPM on heating and cooling temperature exactly matches with the DSC heating and cooling curves.

SEM analysis of chalcone materials

The surface morphological analysis of synthesised crude product of materials **I**, **II** and **III** were examined by Hitachi S 3000H Scanning Electron Microscope (SEM). The SEM analysis is an essential tool to identify the surface morphology of synthesised materials. The synthesised chalcone materials (**I**, **II** and **III**) depicts various morphologies (Fig. 9).

The material **I** establishes ash like uniform morphology similar to the reported literature.[27,28] The micrographs of material **II** exhibits a sphere like morphology and entire surface of molecules were found to be uniform spheres, though the materials **I** and **II** have the similar chemical frame work in molecule the morphology gets differed from each other. It may be due to the presence of carbonyl group (acceptor) occupying different position (Fig. 1). In material **I**, the donor group –OH is very close to the acceptor group (carbonyl) and also the ICT of material **I** is faster than **II**. Hence material **II** attracts other

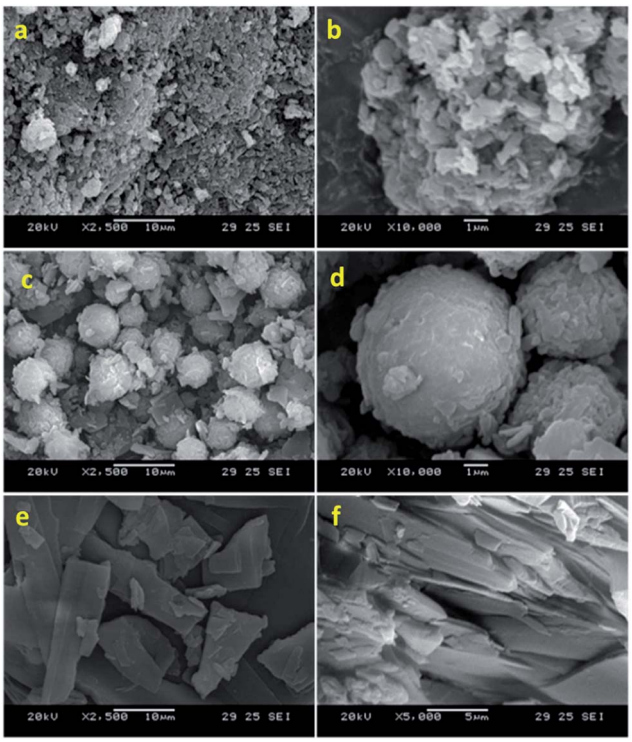

Fig. 9 SEM images of chalcone material I, II and III shown as, (a & b), (c & d) and (e & f) respectively.

molecules slowly, thus exhibiting less agglomeration with sphere like morphology. On the other hand, material **III** has a flat layer like morphology owing to the weak hydrogen bonding in the material.[29] Because of the absence –OH groups, it leads to a less hydrogen bonding in the material prominent to the weak interaction between the molecules resulting in a layered like morphology.

Computational study: DFT calculation

HOMO–LUMO energy gap

The difference between the highest occupied molecular orbital (HOMO) and lowest unoccupied molecular orbital (LUMO) of a neutral system is the easiest way used to calculate excitation energy at its ground state.[30] The HOMO–LUMO energy gap was computed at B3LYP/6-31G (d,p) level basis set using DFT calculation (Gaussian 09). Fig. 10 indicates the HOMO and LUMO energy levels of all the three materials.

The results of the HOMO energy levels of chalcone **I**, **II**, and **III** are −5.76, −5.79 and −5.74 eV. The calculated LUMO energy levels are −1.80, −1.81 and −1.78 eV. The calculated bandgap energy for chalcone **I**, **II** and **III** is as follows 3.96, 3.98 and 3.96 eV. The similar HOMO–LUMO energy gap was obtained for materials **I** and **II** attributable to similar electron clouds, but there is small increase in energy gap was obtained in material **II**, this may be due to the less electronic cloud configuration of the material **II**.

Surprisingly, it is inferred that both **I** and **III** have the same binding energy value. Though all the three materials have

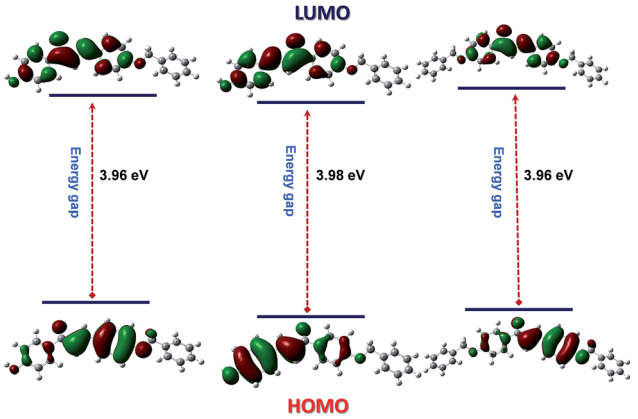

Fig. 10 HOMO and LUMO energy diagram of chalcone I, II and III.

different molecular structure, the overall bandgap is found to be similar for materials **I** and **III**, material **II** shows little higher value. This is attributed to the existence of similar electron clouds present in materials **I** and **III** unlike material **II**. The intra charge transfer of these materials is free of electron motion to the entire molecule. A small variation in the bandgap may be ascribed to the change in the position of functional group present in molecules.

Electrochemical analysis

Corrosion and its application

The corrosion inhibition efficiency of all the three chalcone was studied by potentiodynamic polarization technique. The anodic and cathodic polarization curves (Fig. 11) were obtained in the absence and presence of inhibitors in **I**, **II** and **III**. The corrosion potential (E_{corr}), corrosion current density (I_{corr}), corrosion rate and inhibition efficiency percentage (I.E%) were observed by Tafel plot by extrapolating the anodic and cathodic lines and are listed in Table 2. The following formula (2) is used to find out the corrosion efficiency (I.E%) of the materials.[31]

Corrosion inhibition efficiency

$$\text{I.E\%} = \frac{I'_{corr} - I_{corr}}{I_{corr}} \times 100 \qquad (2)$$

where, I.E% = inhibition efficiency percentage, I'_{corr} = corrosion current density in the absence of inhibitor, I_{corr} = corrosion current density in the presence of inhibitor.

The corrosion efficiency was calculated by using the above eqn (2). The (E_{corr}), (I_{corr}) values and corrosion rate differ much in the presence and absence of the inhibitor. For the prepared samples, the corrosion rate is 20.99 and in the presence of the inhibitor the corrosion rate decreases with respect to concentration of inhibitor materials **I**, **II** and **III**.

I.E% of the all three materials is as follows: material **I** evidenced 85.18% for 10 ppm, 94.14% for 50 ppm and 95.38 for 100 ppm, whereas material **II** exhibited 86.80% for 10 ppm, 95.04% for 50 ppm and 96.33 for 100 ppm, on the other hand,

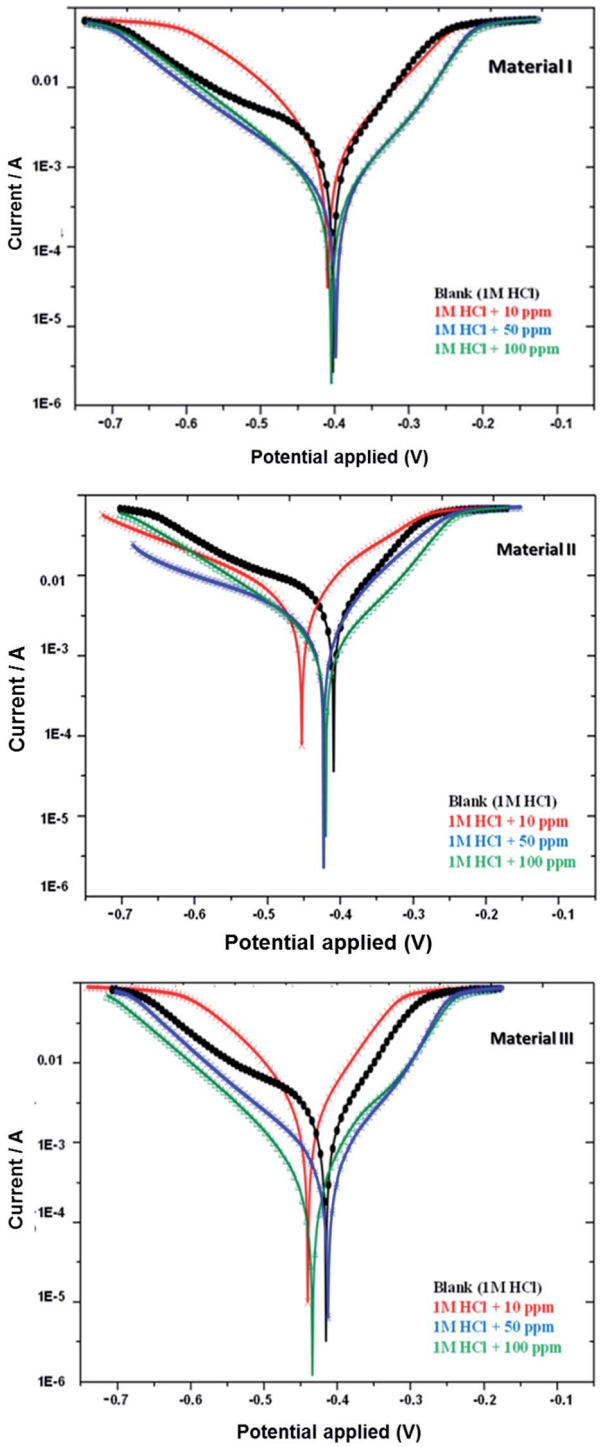

Fig. 11 Tafel plots of inhibitors I, II and III.

material **III** affords 83.13% for 10 ppm, 94.99 for 50 ppm and 97.81 for 100 ppm.

Further increase of inhibitor concentration, there is no significant increase in the I.E%. Therefore, the concentration of 100 ppm was considered as optimum one for all three materials. The entire Tafel polarization curve moves towards the cathodic side. Thus all the three materials act as cathodic inhibitors.[32]

Table 2 Corrosion parameters of chalcone I, II and III

	E_{corr} (mV *vs.* SCE)	I_{corr} (μA cm^{-2})	Corrosion rate (mm per year)	Inhibition efficiency (%)
Chalcone-I				
Blank	−407.61	1080	20.99	—
10 ppm	−413.21	267.69	3.11	85.18
50 ppm	−404.27	106.05	1.23	94.14
100 ppm	−409.38	83.39	0.969	95.38
Chalcone-II				
Blank	−407.61	1080	20.99	—
10 ppm	−448.61	238.03	2.77	86.80
50 ppm	−420.38	89.10	1.04	95.04
100 ppm	−417.46	66.69	0.77	96.33
Chalcone-III				
Blank	−407.61	1080	20.99	—
10 ppm	−430.79	304.81	3.54	83.13
50 ppm	−404.89	90.23	1.05	94.99
100 ppm	−424.84	40.10	0.46	97.81

The maximum efficiencies for 100 ppm obtained from all the three materials are given in Table 2. Among the three compounds, the material **III** demonstrates higher inhibition efficiency in 100 ppm. This reveals that the benzyl group has the more inhibition efficiency than –OH group.

Cyclic voltammetry studies

The cyclic voltammetry analysis reveals the oxidation and reduction properties of the materials. The Fig. 12 displays the oxidation and reduction behaviour of all the three chalcone materials. It is found that all the materials indicate different oxidation states with peaks at the various places 0.85 (eV) for **I**, 1.05 and 1.09 eV for material **II** and **III** respectively. There is no reduction peaks for materials **I** and **III**. But there is a redox peak for **II** at around −0.92 eV, owing to the intra charge transfer which differs from each other with respect to functional group present in the materials. In compound **I**, the ketone group is very close to functional group of phenolic –OH. Thus, it retains less number of free electrons and the oxidation occurs at 0.85 eV. In compound **II**, the free electron is more with respect to extended conjugation of ketone group to the function phenolic –OH group which easily moves away from anodic to cathodic side.

In the case of material **III** the oxidation peak is shifted to 1.09 eV, attributed to more free electrons and there is no phenolic –OH group. Thus, the peak just shifts towards the anodic position. Here the noticeable point is that there is no reduction peaks for materials **I** and **III** but in material **II** there is a redox peak at −0.92 eV which displays the flow of electron and ICT take the role on it. In material **I** the phenolic –OH electron donor group is very close to the electron acceptor C=O carbonyl group. The ICT electron transfer occurs just opposite to the electron flow from the electron donor and acceptor group, once the applied potential consumes both the places. But in the case of **II**, the electron donor, acceptor group and ICT takes place in

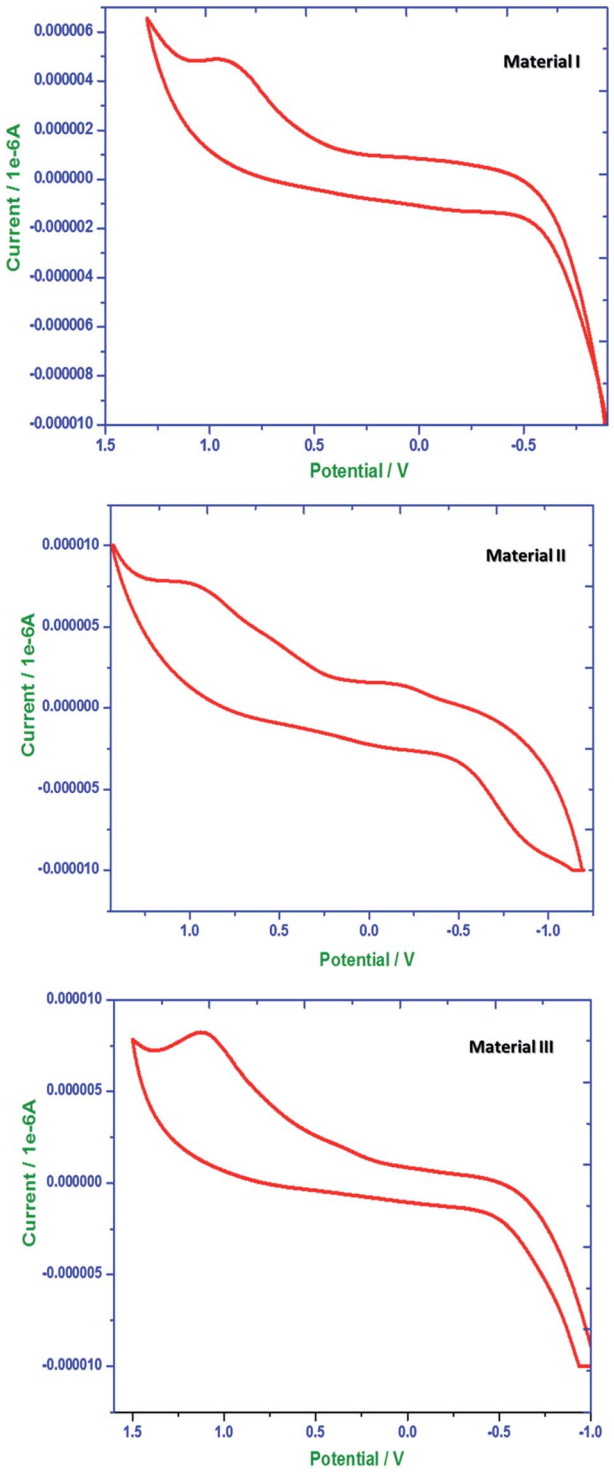

Fig. 12 Cyclic voltammograms of compounds I, II and III.

the same side. It may be the reason for the reduction peak at −0.92 eV. On the other hand, material **III** has no reduction peak due to the absence of electron donor group and also the electron flow once oxidizes the lack of electron donor and it may not be reduced easily.

Photocrosslinking studies

The photo-dimerization of the chalcone materials **I**, **II** and **III** were studied experimentally by ^{1}H-NMR, FT-IR, UV-visible spectrophotometer and microwave photo reactor.[33,34] All the three materials indicate photocrosslinking nature with various time intervals. The crosslinking occurs because of the formation of σ bond from π bond in an organic molecule.[33] In previous report the chalcone enone group (>CH=CH<) were retained at 2π + 2π cyclo addition and the formation of s-*trans* to s-*cis* isomerization occurs,[34] but this materials exhibits photodimerization of the corresponding chalcones which was further confirmed by ^{1}H-NMR and *in situ* FT-IR analysis.[17,35,36] At the end of the crosslinking, materials display fully disappeared π bond and fully formed σ bond.[33]

The photocrosslinking of the materials **I**, **II** and **III** were shown in Fig. 13–15 with various time intervals. The electron donor, acceptor group and ICT lead to a drastic change in photocrosslinking of the molecule.[34] The process occurs here once the molecule gets the energy in the form of UV-light and get excited from the ground state. When all the molecules form σ bond from the π bond it gets saturated and further there is no change in the molecule and it is not reversible. The photocrosslinking formation means σ bond formation mainly depends on the donor, acceptor and intra-charge transfer of the materials.[24] The order of the intra-charge transfer in the materials are as follows **I** > **II** > **III**. The saturation timing of all three materials is 1100, 290 and 33 seconds.

The ^{1}H-NMR spectra of before then after photocrosslinking of compounds **I**, **II** and **III** were shown in Fig. 17–19. From the ^{1}H-NMR spectra, the appearance of peak at 4.2 ppm is due to the formation of cyclobutane ring and the peak disappearance at around 7.4 ppm is due to the deformation of enone (>C=C<) of the corresponding compounds. The peak variations between before and after photo-crosslinking of other protons are may be due to different in the after photo-crosslinking the proton environment. The spectra clearly indicates that all three materials undergone photocrosslinking. The *in situ* photocrosslinkig

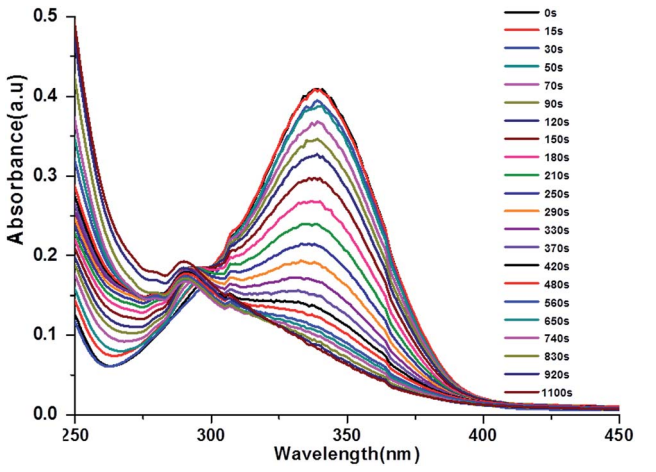

Fig. 13 UV-vis spectra on photocrosslinking of material I upon UV-irradiation at 365 nm with various time intervals.

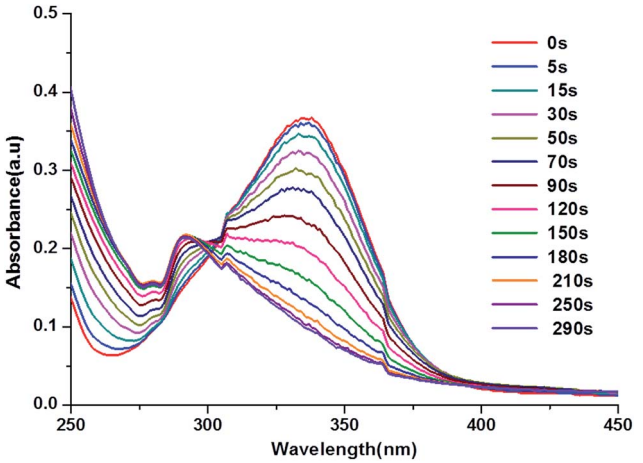

Fig. 14 UV-vis spectra on photocrosslinking of material II upon UV-irradiation at 365 nm with various time intervals.

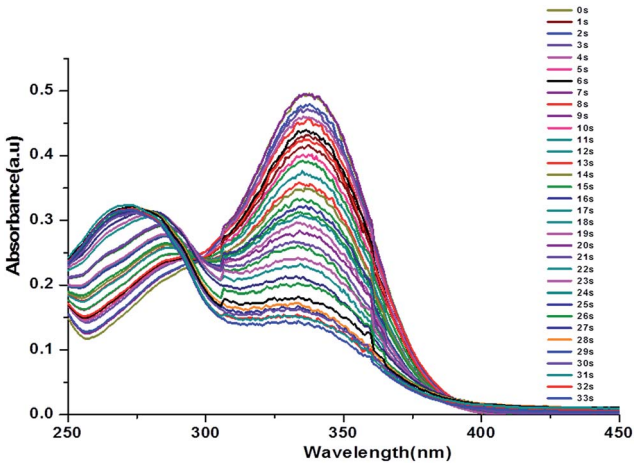

Fig. 15 UV-vis spectra on photocrosslinking of material III upon UV-irradiation at 365 nm with various time intervals.

process was also obtained from FT-IR spectrophotometer as a function of UV-exposure time and shown in Fig. 20. There are significant changes in spectra upon the various UV-irradiation times.[33] The stretching vibration mode of >C=C< (1645 cm^{-1}) decreases while exposing the increase in irradiation time. Simultaneously there are some other spectral changes may be due to the formation of cyclobutane ring. From the above

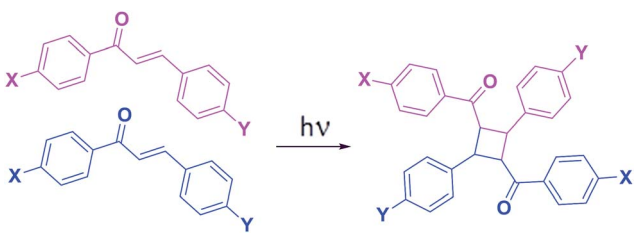

Fig. 16 Structural change upon the UV-irradiation of compounds I, II and III.

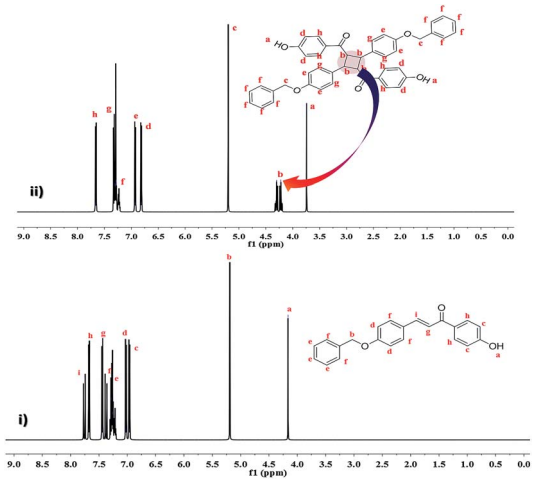

Fig. 17 ^{1}H-NMR spectra on before (i) and after (ii) UV-irradiation of compound I.

results it could understand that the photo-dimerization time of the chalcone compounds may alter with respect to functional group present in a molecule.

In the material **I** the donor –OH group is attached to the acceptor group with bridged phenyl group. This phenolic group tends to compromise the applied energy in the form of photon. The –OH group donates the electrons to the acceptor and delay the excitation of the enone molecule. As a result there is a need of more energy to reach the saturation point in the similar manner, material **II** has a decreased saturation time when compared to **I**.[24] The reason may be the chalcone **II** donor group is attached with the phenyl ring is already involving the ICT. The directly attached donor to the ICT does not give more energy because already occurs delocalization. The donating electrons are decreased from **I** resulting in less saturation time compared to chalcone **III**. In the case of chalcone **III** there is no –OH (donor) group in it, the flow of electrons will be in free motion,

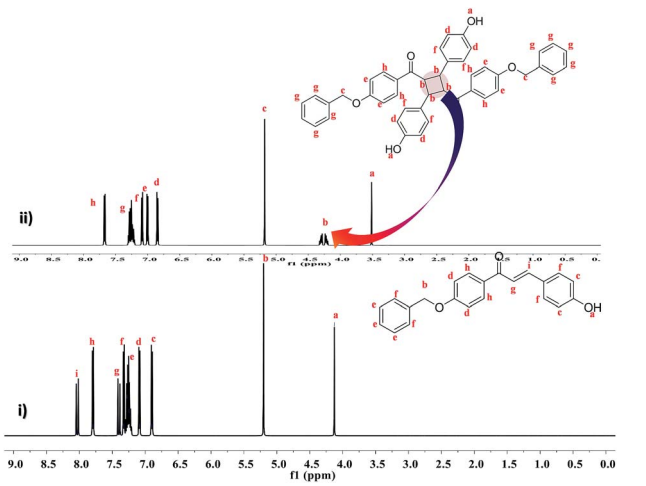

Fig. 18 ^{1}H-NMR spectra on before (i) and after (ii) UV-irradiation of compound II.

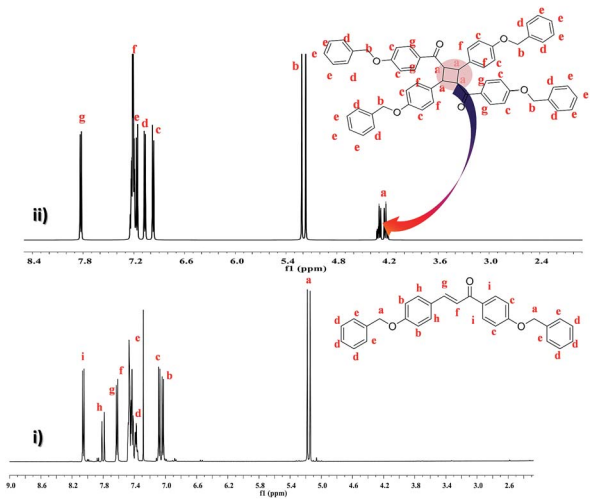

Fig. 19 ^{1}H-NMR spectra on before (i) and after (ii) UV-irradiation of compound III.

within the molecule and it's saturation timing still decreases to 33 seconds. Fig. 16 implies that the general schematic structural changes of chalcone molecule under UV-irradiation photocrosslinking.

Structural nonlinearity relationship and comparative statement

Comparative statement is an important tool to assign similar and dissimilar property of respective group of molecules.[37] The similarity leads to derive various possible compounds and dissimilar statement concludes the change in the molecular pattern in altering the property of molecule.[4] Here, the non centrosymmetric material **I** shows 1.9 times higher SHG efficiency than the reference material: urea. Due to the centrosymmetry nature the materials **II** and **III** have no much SHG response.[4] The position of strong donor acceptor substitution takes a giant role in SHG output. In this molecule there is a carbonyl group (C=O) as an acceptor and a hydroxyl group –OH as a donor for **I**, **II** and for **III** benzyl ether as a weak donor.[36] In material **I**, –OH is close to the acceptor group results in electron delocalization, leads to enhanced SHG efficiency. In case of material **II** contributing charge transfer direction is being from the carbonyl (C=O) group to the hydroxyl (–OH) group.[38] Material **I** is more polar than material **II**. In case of material **III**, the absence of hydroxyl group leads to less polarity nature next to the **II** and **I**. The order of polarity of the materials are given as below **I** > **II** > **III**. The shift in the enone position of the material **I**, **II** and **III** takes a main role in changing the property of the molecule. The ICT of the materials are exposed in Fig. 21. Intra-charge transfer and electron donor acceptor groups present in the compound leads to the change of photocrosslinking timing in different intervals of time.

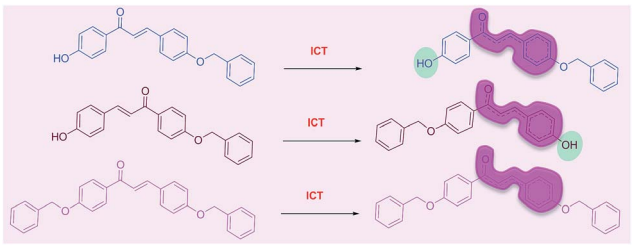

Fig. 21 Possible ICT of compounds I, II and III.

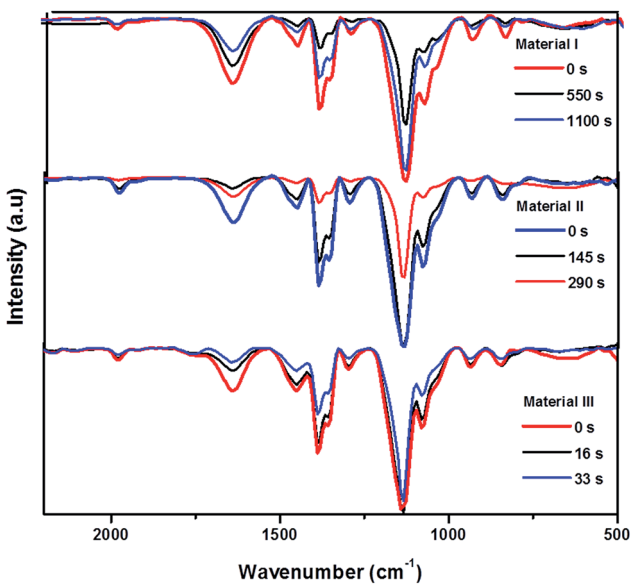

Fig. 20 *In situ* FT-IR spectra of materials I, II and III as a function of UV-irradiation time.

Conclusions

The three different novel chalcone materials have been synthesized and characterized. The surface morphology of these materials was visualized through SEM analysis. Theoretical mode involves HOMO–LUMO calculation of the material from the DFT calculations. The similarity in bandgap energy of the materials was evaluated by theoretical calculation. The thermal properties of material **III** was studied through the HOPM, DSC and TGA analyses. The application studies of these three newly synthesized chalcones were analysed through the corrosion inhibition and photocrosslinking studies. The comparative statement deals about the substitution effect of the chalcone materials. Thus the present investigation helps to study the properties about different combinations of chalcone and its derivatives for different applications.

Acknowledgements

The authors gratefully acknowledge the University Grants Commission, New Delhi, and Government of India for the financial support. Instrumentation facility provided under FIST-DST and DRS-UGC to Department of Chemistry, Anna University are sincerely acknowledged. The authors acknowledge Dr Rajamony Jagan, SAIF, Indian Institute of Technology, Chennai

for the help in X-ray data collection and structure solving. Help rendered by Dr Hubert Joe towards theoretical calculation is greatly acknowledged.

Notes and references

1 S. Vazquez-Rodriguez, R. Figueroa-Guinez, M. Joao Matos, L. Santana, E. Uriarte, M. Lapier, J. Diego Maya and C. Olea-Azar, *Med. Chem. Commun.*, 2013, **4**, 993.
2 H. J. Ravindra, A. John Kiran, S. M. Dharmaprakash, N. Satheesh Rai, K. Chandrasekharan, B. Kalluraya and F. Rotermund, *J. Cryst. Growth*, 2008, **310**, 4169.
3 E. D. D. Silva, G. Krishna Podagatlapalli, S. Venugopal Rao, D. Narayana Rao and S. M. Dharmaprakash, *Cryst. Growth Des.*, 2011, **11**, 5362.
4 V. Ramkumar, S. Anandhi, P. Kannan and R. Gopalakrishnan, *CrystEngComm*, 2013, **15**, 2438.
5 P. Poornesh, S. Shettigar, G. Umesh, K. B. Manjunatha, K. Prakash Kamath, B. K. Sarojini and B. Narayana, *Opt. Mater.*, 2009, **31**, 854.
6 M.-A. Tehfe, F. Dumur, P. Xiao, M. Delgove, B. Graff, J.-P. Fouassier, D. Gigmes and J. Lalevee, *Polym. Chem.*, 2014, **5**, 382.
7 R. Balaji, D. Grande and S. Nanjundan, *React. Funct. Polym.*, 2003, **56**, 45.
8 H. J. Ravindra, W. T. A. Harrison, M. R. Suresh Kumar and S. M. Dharmaprakash, *J. Cryst. Growth*, 2009, **311**, 310.
9 H. R. Manjunath, P. C. RajeshKumar, S. Naveen, V. Ravindrachary, M. A. Sridhar, J. Shashidhara Prasad and P. Karegoudar, *J. Cryst. Growth*, 2011, **327**, 161.
10 A. N. Prabhu, A. Jayaram, K. Subrahmanya Bhat and V. Upadhyaya, *J. Mol. Struct.*, 2013, **1031**, 79.
11 P. S. Patil, M. S. Bannur, D. B. Badigannavar and S. M. Dharmaprakash, *Opt. Laser Technol.*, 2014, **55**, 37.
12 P. S. Patil and S. M. Dharmaprakash, *J. Cryst. Growth*, 2007, **305**, 218.
13 P. S. Patil, S. M. Dharmaprakash, K. Ramakrishna, H.-K. Fun, R. Sai Santosh Kumar and D. Narayana Rao, *J. Cryst. Growth*, 2007, **303**, 520.
14 T.-I. Yang, C.-W. Peng, Y. Li Lin, C.-J. Weng, G. Edgington, A. Mylonakis, T.-C. Huang, C.-H. Hsu, J.-M. Yeh and Y. Wei, *J. Mater. Chem.*, 2012, **22**, 15845.
15 M. Bouklah, B. Hammouti, A. Aouniti, M. Benkaddour and A. Bouyanzer, *Appl. Surf. Sci.*, 2006, **252**, 6236.
16 J. Xu, D. Lai, Z. H. Xie, P. Munro and Z.-T. Jiang, *J. Mater. Chem.*, 2012, **22**, 2596.
17 R. Baskar, D. Kesavan, M. Gopiraman and K. Subramanian, *RSC Adv.*, 2013, **3**, 17039.
18 R. Balaji and S. Nanjundan, *React. Funct. Polym.*, 2001, **49**, 77.
19 P. Wen, Z. Zhong, L. Li, A. Zhang, X.-D. Li and M.-H. Lee, *J. Mater. Chem.*, 2012, **22**, 22242.
20 B. P. Bandgar and S. S. Gawande, *Bioorg. Med. Chem.*, 2010, **18**, 2060.
21 Z. Nowakowska, *Eur. J. Med. Chem.*, 2007, **42**, 125.
22 M. Gopiraman, C. Sathya, S. Vivekananthan, D. Kesavan and N. Sulochana, *J. Mater. Eng. Perform.*, 2012, **21**, 240.
23 N. Sivasankaran and K. Palaninathan, *Polym. Degrad. Stab.*, 2013, **98**, 1852.
24 S. Balamurugan, S. Nithyanandan, C. Selvarasu, G. Y. Yeap and P. Kannan, *Polymer*, 2012, **53**, 4104.
25 K. Y. Li and D. F. Xue, *Chin. Sci. Bull.*, 2009, **54**, 131.
26 K. Sangwal, *Mater. Chem. Phys.*, 2000, **63**, 145.
27 V. Meenatchi, K. Muthu, M. Rajasekar and S. P. Meenakshisundaram, *Phys. B*, 2013, **419**, 95.
28 A. M. Asiri and S. A. Khan, *Mater. Lett.*, 2011, **65**, 1749.
29 K. J. Jarag, D. V. Pinjari, A. B. Pandit and G. S. Shankarling, *Ultrason. Sonochem.*, 2011, **18**, 617.
30 S. Nithyanandan and P. Kannan, *Polym. Degrad. Stab.*, 2013, **98**, 2224.
31 P. Sakunthala, S. S. Vivekananthan, M. Gopiraman, N. Sulochana and A. R. Vincent, *J. Surfactants Deterg.*, 2013, **16**, 251.
32 X. Li, S. Deng and H. Fu, *Corros. Sci.*, 2011, **53**, 3704.
33 D. H. Choi, S. J. Oh, H. B. Cha and J. Y. Lee, *Eur. Polym. J.*, 2001, **37**, 1951.
34 D.-M. Shin, D.-M. Song, K.-H. Jung and Ji-H. Moon, *J. Photosci.*, 2001, **8**, 9.
35 R. Nagwanshi, M. Bakhru and S. Jain, *medicinal chemistry research*, 2012, **21**, 1587.
36 K.-S. Choi, H.-W. Kim, Y.-B. Kim and J.-D. Kim, *Liq. Cryst.*, 2010, **31**, 639.
37 H. P. Avila, E. de Fatima Albino Smania, F. D. Monache and A. S. Junior, *Bioorg. Med. Chem.*, 2008, **16**, 9790.
38 B. Zhao, W. Q. Lu, Z. H. Zhou and Y. Wub, *J. Mater. Chem.*, 2000, **10**, 1513.

